Temperature dependence of current density and admittance in metal-insulator-semiconductor junctions with molecular insulator

Alain-Bruno Fadjie-Djomkam, Soraya Ababou-Girard, R. Hiremath, Cyril Herrier, Bruno Fabre, Francine Solal, Christian Godet

AIP | Journal of Applied Physics

Temperature dependence of current density and admittance in metal-insulator-semiconductor junctions with molecular insulator

A. B. Fadjie-Djomkam, S. Ababou-Girard, R. Hiremath, C. Herrier, B. Fabre et al.

Citation: J. Appl. Phys. **110**, 083708 (2011); doi: 10.1063/1.3651401
View online: http://dx.doi.org/10.1063/1.3651401
View Table of Contents: http://jap.aip.org/resource/1/JAPIAU/v110/i8
Published by the AIP Publishing LLC.

Temperature dependence of current density and admittance in metal-insulator-semiconductor junctions with molecular insulator

A. B. Fadjie-Djomkam,[1] S. Ababou-Girard,[1] R. Hiremath,[1] C. Herrier,[2] B. Fabre,[2] F. Solal,[1] and C. Godet[1,a)]

[1]*Institut de Physique de Rennes, CNRS UMR 6251, Université de Rennes 1, Campus de Beaulieu, Rennes Cedex 35042, France*

[2]*Sciences Chimiques de Rennes, CNRS UMR 6226, Université de Rennes 1, Campus de Beaulieu, Rennes Cedex 35042, France*

(Received 23 June 2011; accepted 7 September 2011; published online 21 October 2011)

Electrical transport in ultrathin Metal-insulator-semiconductor (MIS) tunnel junctions is analyzed using the temperature dependence of current density and admittance characteristics, as illustrated by Hg//$C_{12}H_{25}$ – *n* Si junctions incorporating *n*-alkyl molecular layers (1.45 nm thick) covalently bonded to Si(111). The voltage partition is obtained from $J(V, T)$ characteristics, over eight decades in current. In the low forward bias regime (0.2–0.4 V) governed by thermionic emission, the observed linear *T*-dependence of the effective barrier height, $q\Phi_{EFF}(T) = q\Phi_B + (kT)\beta^0 d_T$, provides the tunnel barrier attenuation, $\exp(-\beta^0 d_T)$, with $\beta^0 = 0.93$ Å^{-1} and the thermionic emission barrier height, $\Phi_B = 0.53$ eV. In the high-forward-bias regime (0.5–2.0 V), the bias dependence of the tunnel barrier transparency, approximated by a modified Simmons model for a rectangular tunnel barrier, provides the tunnel barrier height, $\Phi_T = 0.5$ eV; the fitted prefactor value, $G_0 = 10^{-10}$ Ω^{-1}, is four decades smaller than the theoretical Simmons prefactor for MIM structures. The density distribution of defects localized at the $C_{12}H_{25}$ – *n* Si interface is deduced from admittance data (low-high frequency method) and from a simulation of the response time $\tau_R(V)$ using Gomila's model for a non equilibrium tunnel junction. The low density of electrically active defects near mid-gap ($D_S < 2 \times 10^{11}$ eV^{-1}.cm^{-2}) indicates a good passivation of dangling bonds at the dodecyl – *n* Si (111) interface. © *2011 American Institute of Physics*. [doi:10.1063/1.3651401]

I. INTRODUCTION

Hybrid semiconductor—organic molecular layers (OMLs) devices combine the advantages of semiconductor (SC) technology (doping, processing) and offer wide opportunities to incorporate molecular functionalities for bio-sensing and nano-electronics.[1–3] The development of metal-insulator-semiconductor (MIS) junctions with ultrathin insulator ($d_T < 3$ nm) has stimulated the study of new insulating materials, such as high band gap saturated organic chains which are expected to suppress hopping of charge carriers within electronic states localized along the molecule.[4]

Covalently bound linear saturated (*n*-alkyl) chains form robust molecular layers with a high coverage and play the role of a nanometer-thick tunnel barrier (TB); however, steric molecular constraints do not allow a full passivation of Si(111) surface sites which remain subject to post-grafting oxidation at the ambient.[5–7] Electrical transport properties of hybrid M–OML–SC devices have been widely studied[8–19] due to their relatively low density of electrically active defects at the OML—Si interface.[20–23]

Analysis of current-voltage (*I-V*) characteristics of molecular MIS tunnel junctions (M–OML–SC) is still a controversial topic due to the simultaneous contribution of different mechanisms (tunneling, thermionic emission (TE), and generation-recombination) potentially involved in the transport of electrical charge carriers, in addition to some influence of series resistance at high current density. Several methods were proposed to analyze the direct current (dc) transport properties,[8–19] however, most studies were performed only at room temperature. In spite of some efforts to combine tunneling and thermionic emission transport through weighting parameters with little physical basis,[14,15] there is no clear method to evaluate the contribution of a thin ($d_T = 1-2$ nm) molecular tunnel barrier in the regime where both mechanisms contribute to the current. The tunnel attenuation parameter, $\beta^0 d_T$, is usually obtained at room temperature using junctions grafted with variable chain length (d_T); however the structure dependent β^0 values in these "nominally identical" junctions may be affected by different coverage or structural ordering.[8]

In this work, we show that the *temperature dependence* of current density, $J(V, T)$, characteristics is crucial to describe the different mechanisms which contribute to charge transport through rectifying MIS junctions with a molecular insulator. In the energy band diagram of a metal–semiconductor system with a thin interfacial insulator layer, a partition of the dc applied voltage, $V = V_{DC}$, occurs between the tunnel barrier and the space charge in the semiconductor (Fig. 1). The main junction parameters are the thickness of the insulator layer (d_T), the work function of the metal ($q\Phi_M$), the electron affinity of the semiconductor (qX_{Si}), the potential drop across the

a)Author to whom correspondence should be addressed. Electronic mail: christian.godet@univ-rennes1.fr. Present address: EPSI—IPR (Bât. 11C—Beaulieu), Université Rennes 1, 35042 Rennes, France.

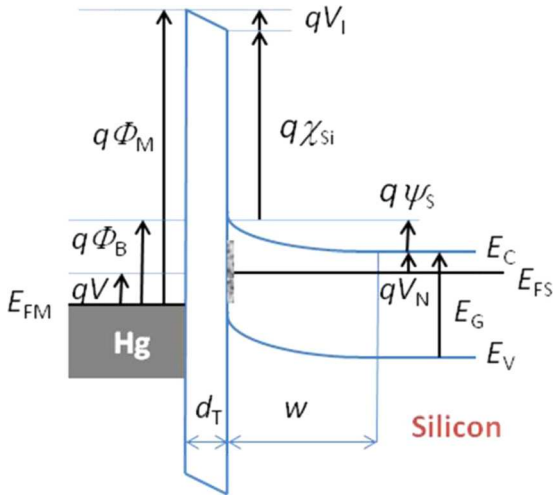

FIG. 1. (Color online) Band diagram of the Hg—OML—*n* Si(111) tunnel MIS junction under small forward bias.

interfacial layer (V_I), and the surface potential (Ψ_S). While all of the experimental data presented in this work were obtained using Hg//$C_{12}H_{25}$ – *n* Si (111) junctions incorporating densely packed *n*-alkyl (C_{12}) molecules, the method to obtain the voltage partition from $J(V, T)$ is more general and could be applied to any rectifying tunnel MIS device.

Since a modulation of the applied voltage, $V + V_{AC}\exp(j\omega t)$, drives a modulation of current through different parts of the MIS tunnel junction, admittance spectroscopy is helpful to discriminate transport mechanisms with different sensitivities to the ac modulation of the interface potential, Ψ_S. Hence, besides $J(V, T)$ measurements in the T range 243–293 K, the admittance $Y(V, T, \omega)$ was characterized in a wide frequency range (10^{-2} to 10^7 Hz) in order to investigate the dynamic characteristics of the tunnel barrier, the space charge region, and the interface traps. In densely packed monolayers, although the molecules self-organize through intermolecular van der Waals interactions, wide bandgap saturated molecules are not expected to be electrically active; the very small dipolar relaxation effects in response to an external ac field are beyond the scope of this paper.

Section II describes the experimental methods, including photochemical grafting, x-ray photoelectron spectroscopy (XPS) characterization of OML coverage, spectroscopic ellipsometry (SE), and dc and ac electrical transport. A specific sample holder compatible with a Hg electrode has been developed for this investigation of transport mechanisms at variable T. Section III reports the current density $J(V, T)$ and admittance $Y(V, T, \omega)$ characteristics measured as a function of temperature, T, angular frequency, ω, and dc voltage, V; here, admittance spectroscopy is used to obtain the flat band voltage, V_{FB}, the device response time, τ_R, and the density of interface electronic states, D_S. In Sec. IV, a method is proposed to describe self-consistently the different mechanisms which contribute to dc charge transport through M–OML–SC junctions in a wide forward bias range. In the low-forward-bias regime (0.2–0.4 V) governed by thermionic emission, the linear T-dependence of the effective barrier height provides the tunnel barrier attenuation, $\exp(-\beta^0 d_T)$, and the thermionic emission barrier height, Φ_B. In the high-forward-bias regime (0.5–2.0 V), the bias dependence of the tunnel barrier transparency is approximated by a modified Simmons model[24] for a rectangular tunnel barrier; it provides the tunnel barrier height Φ_T and a prefactor, G_0, related to the tunneling probability. The bias-dependence of the apparent ideality factor derived from $J(V, T)$ data is discussed in terms of a distribution of barrier heights. Finally, the density distribution of defects localized at the $C_{12}H_{25}$ – *n*-Si interface is deduced from admittance data using a non equilibrium tunnel junction model.[25,26]

II. EXPERIMENTAL

A. Grafting process

Covalent grafting of linear alkene molecules was performed on hydrogenated Si(111):H surfaces with a low miscut angle (<0.5°) using a UV-assisted liquid phase process. A low-doped *n*-type Si (1-10 Ω cm, Siltronix) has been chosen to obtain rectifying junctions;[11,14] however the doping level should not be too high in order to limit the silicon oxidation reaction during the liquid phase grafting process.[27]

Before grafting, the surface of a single side polished *n*-type Si(111) substrate was cleaned in successive ultrasonic baths of acetone (MOS semiconductor grade, Carlo Erba), ethanol (99.8%, VLSI semiconductor grade), and ultrapure 18.2 MΩ cm water (Elga Purelab Classic UV, Veolia Water STI). Organic decontamination was performed in 3:1 v/v concentrated H_2SO_4/30% H_2O_2 at 100 °C for 30 min, followed by copious rinsing with ultrapure water. The surface was etched at room temperature (15 min) with argon-deaerated 40% aqueous NH_4F (semiconductor grade, Riedel-de-Haën), then rinsed with argon-saturated water and blown dry with argon.[28] This fully hydrogen-passivated Si(111):H surface is hydrophobic (water contact angle of 84°) and free of C and O contamination, as shown by XPS.

Before the grafting step, liquid alkene was passed through a neutral, activated alumina column to remove residual water and peroxides. Si(111):H surfaces were transferred into a Pyrex Schlenk tube containing ca. 7–8 ml of alkene reactant, previously deoxygenated at 100°C for 2 h. Dodecyl monolayers were prepared from the photochemical reaction at 300 nm for 3 h of Si(111):H with 1-dodecene (puriss, >99%, Fluka).[29,30] The covalently modified surface was rinsed with distilled CH_2Cl_2, then dipped in hot acetic acid at 65°C (2 × 20 min),[31] and dried under an Ar stream before characterization by XPS, SE, and electrical transport measurements.

B. X-ray photoelectron spectroscopy

The alkyl molecular coverage (Σ_{ML}) and unintentional silicon oxidation were characterized by XPS after a few minutes exposure to the ambient,[30] using a Mg Kα (1253.6 eV) anode source and Omicron HA100 electron energy analyser (1.0 eV resolution). The thickness, d_{OML}, of the molecular layer immobilized on the Si surface was derived from the attenuation $[\text{Si } 2p]_{grafted}/[\text{Si } 2p]_{bare} = \exp(-d_{OML}/\lambda_{OML}\cos\theta)$, with an

inelastic mean free path value $\lambda_{OML} = 3.5$ nm (for Si2p photoelectrons) typical of a dense molecular layer.[32,33]

C. Spectroscopic ellipsometry

SE experiments were performed in the range from 1.0 to 4.7 eV, at an incidence angle of 70°, using a Horiba (UVISEL) ellipsometer and analyzed with a multilayer model. To describe the dielectric function of the OML, an energy independent refractive index was chosen because no improvement in the fitting result was found with a dispersion formula. The optical thickness, d_{SE}, values were derived using a refractive index $n_{SE} = 1.48$.

D. Electrical transport measurements

Molecularly modified surfaces were probed using a mercury top electrode (contact area $S = 5 \times 10^{-3}$ cm^2) to avoid electrical shorts through pinholes in the OML. Figure 2 shows the home-made parallel plate Teflon cell, compatible with Hg, used for current density $J(V, T)$ and admittance $Y(V, T, \omega)$ measurements. The top contact to the OML was taken through a Pt wire and a fresh Hg drop (99.999% Fluka). An ohmic back contact was made by applying a silver paste electrode on the scratched Si backside. Dc and ac transport measurements were performed in a cryostat under dry nitrogen flow to avoid water condensation and to minimize surface oxidation during the measurements. $J(V)$ characteristics were measured in the dark, at several locations of the fresh device, using a Keithley 6487 picoammeter; voltage ramps were progressively increased in the range 0/+2 V and 0/−4 V, using alternatively positive and negative polarities.

Admittance measurements were carried out with a frequency response analyzer (Alpha-A High Resolution measurement system, Novocontrol Technologies). The sample holder was inserted in a two terminal active cell with the impedance converter mounted directly above the sample. Since no V_{AC}-dependence was observed in the range 0.1-20 mV, the ac voltage amplitude was set at $V_{AC} = 10$ mV. Experiments were carried out in two runs: a voltage sweep (waiting time 0.3 s/step 25 mV) and a frequency sweep (13 points per decade in the range 1×10^{-2} Hz to 1×10^{7} Hz), to study the measured complex admittance, $Y(V, T, \omega) = G_m + j\omega C_m$, against voltage, V, and frequency, $\omega/2\pi$. The Teflon cell capacitance ($C_{PAR} = 4.5$ pF) was subtracted to obtain C_m.

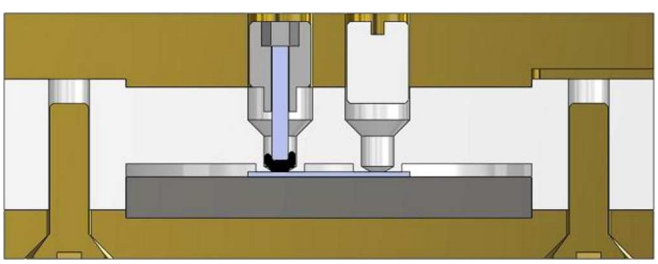

FIG. 2. (Color online) Parallel plate sample holder for transport measurements. The top contact to the OML is taken through the vertical Pt wire and the 0.8 mm diameter Hg drop (black) while the Si backside is contacted with Ag paste. The empty Teflon cell (grey part) contributes to a parasitic capacitance $C_{PAR} = 4.5$ pF.

High frequency and high forward bias admittance data were corrected for the series resistance, R_S, due to bulk Si and back contact resistance. At each temperature, R_S can be derived either from a full analysis of $J(V_{DC})$ (Sec. IV B) or from the high frequency value of the real part of the impedance, $R_S = G_m/(G_m^2 + \omega^2 C_m^2)$.[34] This R_S-correction does not affect the interface density of states or flat band voltage analysis and it decreases the response time by a factor of less than 2.

III. RESULTS

In this study, no SiO_2 component could be observed near 103 eV on Si2p spectra taken at $\alpha = 45°$ immediately after dodecyl grafting. The optical thickness $d_{SE} = 1.45$ nm and the molecular coverage $\Sigma_{ML} = 2.3 \times 10^{14}$ cm^{-2} (Table I) both indicate grafting of a rather dense C_{12} monolayer. Current density $J(V, T)$ and admittance $Y(V, T, \omega)$ characteristics of Hg//$C_{12}H_{25}$ – n Si(111) junctions are reported in their as-grafted state. The hypothesis and methods used to derive the applied voltage partition, barrier heights, response times τ_R, and energy distribution of interface states $D_S(E_C - E_T)$, are described below.

A. Dc current density

Direct current characteristics $J(V, T)$ of Hg//$C_{12}H_{25}$ – n-Si junctions show a strong rectification which increases with decreasing temperature (Fig. 3). The forward (reverse) regime is obtained for a positive (negative) voltage applied on Hg. The rectification ratio $R = J_{FWD}(V)/J_{REV}(-V)$ values at ±1 Volt is larger than 10^6, being essentially limited by R_S in the forward regime ($V > 1.5$ V).

At low forward bias ($0 < V < 0.4$ Volt), an exponential $J(V)$ dependence is observed for all temperatures. The ideality factor ($n = 1.45$) which describes this slope is similar to previous molecular—n Si junctions.[10,11] As discussed in Sec. IV B, these results will be described by a TE mechanism. At high forward bias ($V > 0.6$ V), saturation in $J(V)$ and weak temperature dependence of $J(T)$ indicate that the current becomes limited either by the TB or by some contact resistance, rather than by the TE barrier inside the semiconductor. This behavior is typical of rectifying MIS tunnel junctions obtained previously with Hg//OML – n type Si.[10–12,14]

In the reverse bias range, Fig. 3 shows that the current depends strongly on temperature with an apparent activation energy $E_{ACT}(J_{REV}) \approx 0.58 \pm 0.05$ eV. For this oxide-free junction, the reverse current density $J(V)$ is remarkably flat, in contrast with oxidized interfaces (not shown) where a larger slope is attributed to Si-SiO_x interface states. The bias dependence of the reverse current is discussed in Sec. IV C.

B. Admittance measurements

Complex admittance $Y^*(\omega) = G + j\omega C$ (for a parallel R-C circuit) as a function of the angular frequency, $\omega = 2\pi f$, may be analyzed using related complex formalisms: the impedance $Z^* = Y^{*-1}$, the permittivity ε^*, and the modulus $M^* = (\varepsilon^*)^{-1}$. In this work, we will use the capacitance $C(V)$ to obtain the flat band voltage, the modulus $M(\omega)$ to derive

TABLE I. Optical thickness d_{SE} (SE) and molecular coverage Σ_{ML} (XPS) of the $C_{12}H_{25}$ molecular layer. Electrical characteristics of the Hg//$C_{12}H_{25}$ – *n* Si junction: ideality factor, *n*, effective barrier height, Φ_{EFF} (293 K), attenuation parameter, $\beta^0 d_T$, flat band voltage, V_{FB}, interface density of states, D_S, and response time τ_R (293 K).

	SE	XPS	$J(V,T)$			$Y(\omega,V,T)$		
OML	d_{SE} (nm)	Σ_{ML} (10^{14} cm^{-2})	*n*	Φ_{EFF} (eV)	$\beta^0 d_T$	V_{FB} (V)	D_S (10^{11} cm^{-2}eV^{-1})	τ_R (s)
nSi-C12	1.45	2.3	1.45	0.87	13.5	+0.68	0.1–2.0	1×10^{-7}–0.3

the junction response time, $\tau_R = (C/G)$, and the capacitance $C(\omega)$ to estimate the density of interface states, D_S.

A first evaluation of the quality of the Hg//$C_{12}H_{25}$ – *n*-Si junction is given by the capacitance hysteresis in a cyclic voltage scan. A typical $C(V)$ scan, with 25 mV step and 0.3 s waiting time, was obtained from 0 V to −4 V (depletion) to +0.8 V (accumulation near flat band conditions) to 0 V. Immediately after grafting, Figure 4(a) does not show detectable hysteresis at any frequency (from 10^2 Hz to 10^6 Hz). It has also been checked that the range of *V* bias applied to the device does not change irreversibly the admittance characteristics; the shift of the flat band voltage remains smaller than 0.1 eV after forward biasing at $V=+1$ V ($J=0.05$ A.cm^{-2}) for 30 s.

As shown in Fig. 4(a), the capacitance at reverse bias ($V<0$ V) is low, $C_{REV}=$ 10-20 pF (2-4 nF.cm^{-2}), at all frequencies, showing the formation of a depletion layer. It has been suggested that an inversion layer does not form because the hole tunnelling time is expected to be shorter than the generation-recombination time.[36] In weak depletion (+0.2 V $< V <$ +0.7 V), $C(V)$ data reveal a strong frequency dependence which indicates the additional contribution of interface states at lower frequencies; in the equivalent circuit (inset Fig. 4(a)), they correspond to a parallel (R_{IT}//C_{IT}) component. The measured low frequency capacitance in the forward bias range is larger than the geometric capacitance value of the molecular insulator, $C_I=9$ nF, expected from $d_{SE}=1.45$ nm, $S=5\times10^{-3}$ cm^2, and $\varepsilon_I=3$ (Ref. 10); this result is specific of ultrathin tunnel MIS junctions (low R_T value of the tunnel barrier in the equivalent circuit, inset Fig. 4(a)), as discussed in Sec. IV D.

The Mott-Schottky plot (Fig. 4(b)) of the Hg//$C_{12}H_{25}$ – *n* Si junction shows a linear dependence of C^{-2} vs *V*, as expected when the space charge layer capacitance is much smaller than the insulator capacitance C_I (Eq. (3)). The *V*-axis intercept at high frequency (1 MHz and 100 kHz) yields the flat band voltage value, $V_{FB}=0.68\pm0.03$ V. This value is consistent with previous results.[10,12,16] The doping density, $N_D=1.5\pm0.5\times10^{14}$ cm^{-3}, provides the position of the bulk Fermi level, $(E_C-E_{FB})=qV_N=kTLn(N_C/N_D)=0.306$ eV at 293 K (0.252 eV at 243 K), where $N_C(\text{cm}^{-3})=2.8\times10^{19}\,(T/300)^{1/2}$ is the effective density of states in the Si conduction band. In Sec. IV B, the barrier $q\Phi_B^C$, derived from V_{FB}, will be compared with $q\Phi_B^J$, derived from $\Phi_{EFF}(T)$ in dc transport.

For a parallel *R-C* circuit, the response time, $\tau_R=(C/G)$, is the ratio of the capacitance to the conductance; $\tau_R=\omega_{MAX}^{-1}$ is the inverse angular frequency at the

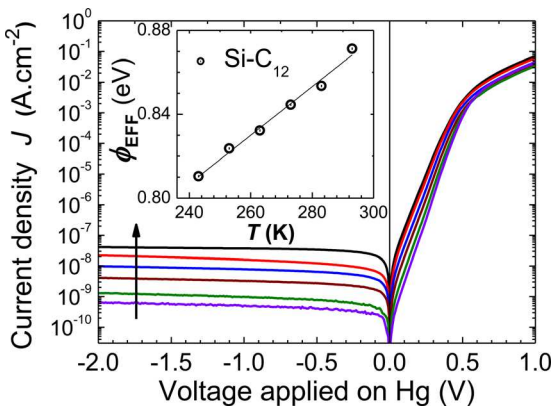

FIG. 3. (Color online) Temperature dependence of current density $J(V)$ characteristics (Hg//$C_{12}H_{25}$ – *n*-Si junction) in the range 243-293 K (step 10 K). Inset: effective barrier height, $\Phi_{EFF}(T)$, derived in the forward bias 0.1-0.3 V range.

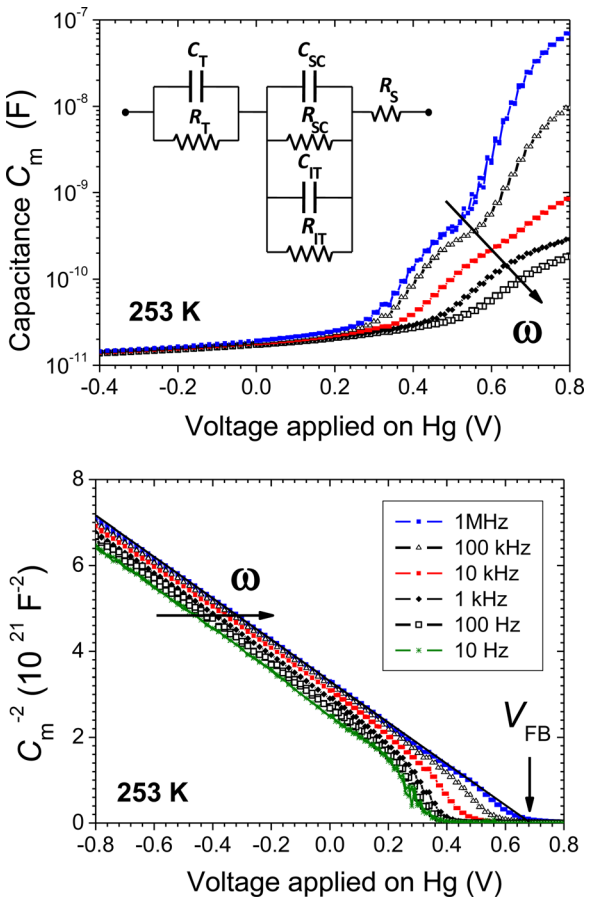

FIG. 4. (Color online) Frequency dependence of the measured capacitance of a Hg//$C_{12}H_{25}$ – *n*-Si junction at $T=253$ K: (a) $C_m(V)$ from 100 Hz to 1 MHz showing the absence of hysteresis and (b) Mott-Schottky plot (C_m^{-2} vs V) giving the flat band voltage.

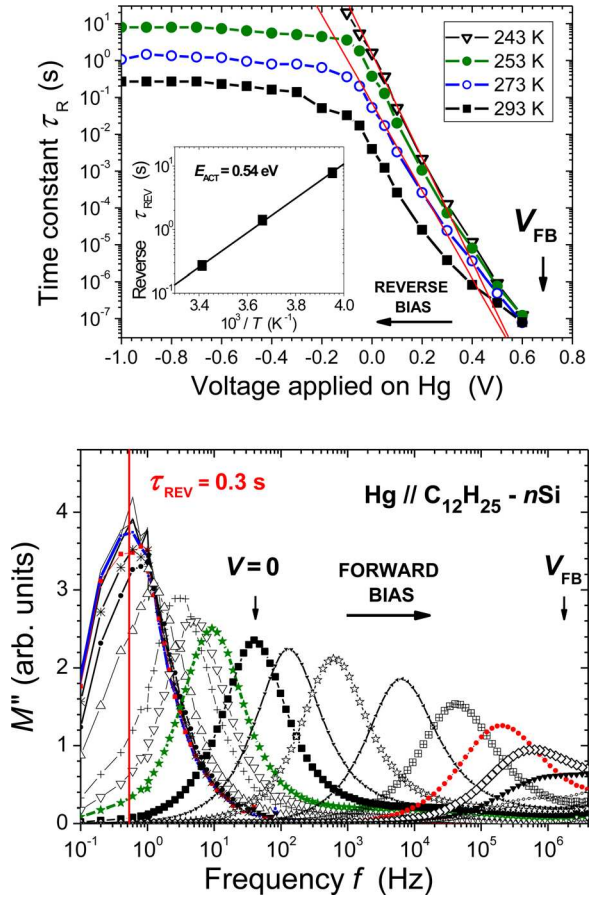

FIG. 5. (Color online) (a) V-dependence of the junction response time, τ_R. Inset: Arrhenius plot of τ_R in the reverse bias regime (−0.8 V). (b) Modulus M'' vs $(\omega/2\pi)$ plot at 293 K.

maximum of $Z''(\omega)$ (not shown) or $M''(\omega)$ plots (Fig. 5(b)). Figure 5(a) shows that the response time of the Hg//$C_{12}H_{25}$ – n-Si junction covers more than eight decades, with an exponential $\tau_R(V)$ dependence, $\tau_R = \tau_R^* \exp(-qV/n_R kT)$, in the same range as the exponential $J(V)$ plot. It is found that $n_R = 1.45$ for all temperatures; within experimental errors, this value is equal to the ideality factor, n, of the $J(V)$ plot. At 293 K, a clear saturation of $\tau_R \approx 0.3$s is observed in the reverse bias regime. This saturation value increases strongly with decreasing T with an activated behavior; an Arrhenius plot $\tau_R = \tau_R^0 \exp(E_{ACT}/kT)$ provides $E_{ACT} = 0.54$ eV and $\tau_R^0 = 1.5 \times 10^{-10}$ s (Fig. 5(a), inset). In contrast, the T dependence of τ_R vanishes as the junction is biased near the flat band voltage, $V_{FB} = 0.68$ V, where extremely small response time values ($\tau_R \approx 100$ ns) are obtained (Fig. 5(a)).

IV. DATA ANALYSIS AND DISCUSSION

The band diagram of the tunnel MIS junction (Fig. 1) is briefly described in order to analyze the dc and ac transport characteristics, in relation with the voltage drop on the insulator and the density of states at the molecular insulator/SC interface.

A. Band diagram of the tunnel MIS diode

For a given applied voltage bias, V, applied to the metal, the admittance and the current density characteristics refer to the same distribution of potential profile defined by the condition of a uniform dc current density across the junction and Gauss law for the distribution of charges in the space charge region (Q_{SC}) and at the interface traps (Q_S). In the tunnel MIS diode band diagram, the actual barrier height (Φ) may differ from the built-in potential because of the change in potential across the molecular layer (V_I) due to molecular capacitive effects and change in potential across the first few atomic layers at the Si surface due to interface charge (Q_S). This interface charge density, positive or negative, influences the unequal distribution of the applied bias, V, between the semiconductor and the insulating layer.

The junction is defined by the metal work function ($q\Phi_M$), the electron affinity (qX_{Si}) and band gap (E_G) of silicon, the bulk Fermi level position (E_{FB}) relative to the conduction band, $qV_N = E_{CB} - E_{FB}$, and the interface band bending, $q\Psi_S(V) = E_{CS}(V) - E_{CB}$ (positive for reverse bias, $V < V_{FB}$, and n-type Si). An effective electron affinity $(qX_{Si})_{EFF}$ may result from dipoles at the OML-Si interface after grafting. Using Gauss law and assuming that the equilibrium potentials are not significantly modified by the large current density through the device, the potential drop across the insulator is represented by

$$V_I(V) = (\Phi_M - X_{Si})_{EFF} - \Psi_S(V) - V_N - V = \frac{d_T}{\varepsilon_I}(Q_S + Q_{SC}), \quad (1)$$

where ε_I is the permittivity of the insulator. For a reverse biased junction, the capacitance of the depletion layer, $C_{SC} = \frac{dQ_{SC}}{d\psi} = \varepsilon_0\varepsilon_S/w$, is modelled by a parallel-plate capacitor with thickness equal to the depletion width $w = (2\varepsilon_0\varepsilon_S\Psi_S/qN_D)^{1/2}$: $Q_{SC} = qN_D w = (2q\varepsilon_0\varepsilon_S N_D \Psi_S)^{1/2}$ where ε_S is the permittivity of silicon. For the low-doped Si used in this work, the space charge density $Q_{SC}(V)$ is comparable to $Q_S(V)$ if $D_S \approx 2 \times 10^{10}$ cm^{-2} eV^{-1}. Hence, V_I is positive in the reverse bias regime ($V < 0$, $Q \approx Q_{SC} > 0$) and V_I is negative in the forward bias regime near the flat band voltage ($V \approx V_{FB}$, $Q \approx Q_S < 0$). Setting $(d\Psi_S/dV) = -1/n$, the barrier height (Fig. 1) is given by

$$\Phi_B = \Psi_S(V) + V + kT/q + V_N, \quad (2a)$$

$$\Phi_B^C = (1/n)V_{FB} + V_N, \quad (2b)$$

where the applied voltage, V_{FB}, at flat bands ($\Psi_S(V_{FB}) = 0$) is obtained from the V-axis intercept in the Mott-Schottky plot of C^{-2} vs V (Fig. 4(b)) using

$$\frac{1}{C^2} = -\frac{2(qV - qV_{FB} - kT)}{q\varepsilon_0\varepsilon_S N_D S^2}. \quad (3)$$

In the reverse bias regime, occupied interface states near the surface Fermi level are localized deeply below the semiconductor conduction band and are more likely in equilibrium with the metal Fermi energy. Hence, as a result of a distribution of interface states in space and in energy, one may consider that a fraction (D_{SA}) is in equilibrium with the metal and a fraction (D_{SB}) is in equilibrium with the semiconductor.[37] Equation (2) gives

$$\alpha = n - 1 = \frac{(\varepsilon_S/w) + qD_{SB}}{(\varepsilon_I/d_T) + qD_{SA}}, \quad (4)$$

showing that the ideality factor is expected to increase (decrease) as D_{SB} (D_{SA}) increases. In reverse bias, $n \approx 1$ since $\varepsilon_I d_T \gg \varepsilon_S w$ and D_{SB} can be neglected, while in forward bias $n - 1 = \frac{qD_{SB}}{(\varepsilon_I/d_T)+qD_{SA}} \approx qD_{SB}d_T/\varepsilon_I$. For large current densities (non-equilibrium condition), a more realistic model using coupled kinetic equations predicts a similar behaviour for $n(V)$.[25]

These models assume homogeneous interface properties; they qualitatively match the experimental bias dependence of the apparent ideality factor, $n(V)$, in the Hg//$C_{12}H_{25}$ – *n* Si junction as shown in Fig. 6(a) where $(q/n(V)\ kT)$ was obtained from a derivation of Ln[$J(V)$/(1–exp($-qV/kT$))] vs V. Interestingly, n is equal to unity in the reverse bias regime, independent of temperature, and it increases steadily in the forward bias range until a plateau value is reached in the range $0.2 < V < 0.4$ Volt. As expected, the plateau value in $n(V)$ is equal to the average inverse slope n_{AV} (arrow in Fig. 6(a)) obtained in the exponential regimes of Ln $J(V)$ (Fig. 3) and Ln$\tau_R(V)$ (Fig. 5(a)). In contrast with the sharp transition in the calculated $n(V)$,[25] a broad transition region is obtained in the experimental $n(V)$; this broadening can be tentatively attributed to a distribution of effective barrier heights due to local potential fluctuations (dipoles or charged defects).

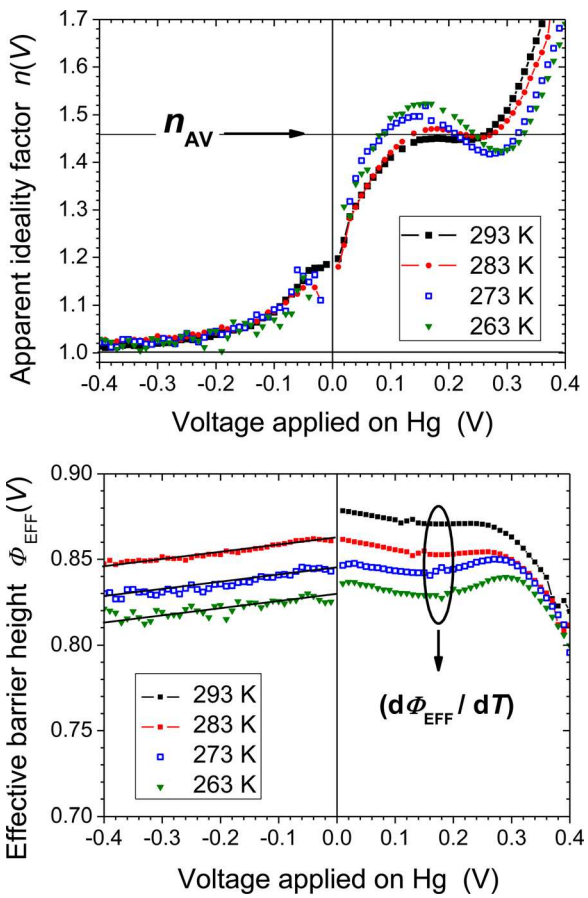

FIG. 6. (Color online) Ideality factor $n(V)$ and effective barrier height $\Phi_{EFF}(V)$ derived from $J(V)$ at 293 K, 283 K, 273 K, and 263 K, using Eq. (5).

The stronger oscillation in $n(V)$ which appears at lower T (Fig. 6(a)) is consistent with a larger relative contribution of low barrier patches in the junction.[38–40]

The effective barrier height $q\Phi_{EFF}(V)$ was derived in the TE approximation using $n(V)$ and Eqs. (5) and (6). The T-dependence of $q\Phi_{EFF}$ will be discussed in Sec. IV B (Eq. (6)). At a given T value, the variations in $q\Phi_{EFF}(V)$ are small in reverse bias and moderate forward bias ($V < +0.3$ V). At higher forward bias, $n(V)$ and $\Phi_{EFF}(V)$ depart from their plateau value because a large fraction of the applied bias is dropped on the insulator and a full analysis of the voltage partition is required.

B. Analysis of the forward current density

In this section, the voltage partition of the Hg//$C_{12}H_{25}$ – *n* Si junction is derived in the forward bias regime. The exponential $J(V)$ at low forward bias ($0.1 < V < 0.4$ Volt) is described by a thermionic emission mechanism above the barrier Φ_B. For a Schottky barrier at a semiconductor metal-interface,[39,41] with a barrier height, Φ_B, and ideality factor, n, the current is

$$I(V) = A^*ST^2\exp(-\beta^0 d_T)\exp(-q\Phi_B/kT)\exp(qV/nkT) \times [1 - \exp(-qV/kT)], \quad (5)$$

where the tunnel barrier transparency $\exp(-\beta^0 d_T)$ has been included; A^* is the Richardson constant ($A^* = 112$ A.cm^{-2}.K^{-2} for *n*-type Si), q the electron charge, k the Boltzmann constant, T the temperature, and S the Hg drop contact area. In the interfacial layer—thermionic—diffusion model of Wu,[42] a quasi-Fermi potential $\Phi_n(x)$ associated to the current flow has been introduced along with the thermal velocity (V_R) and an effective diffusion velocity (V_D); for large $\beta^0 d_T$ values (which is the case with $\beta^0 d_T = 13.5$ for the C_{12} barrier in this work), $\exp(-\beta^0 d_T) \ll (V_D/V_R)$, hence $J(V)$ reduces to the interfacial layer—thermionic model (Eq. (5)).[43]

The slope of LnJ vs V gives the ideality factor value, $n = 1.45$ at 293 K increasing towards $n \approx 2$ at lower temperatures. As in Schottky devices, a Ln(I_S/T^2) *vs* $1/T$ plot is linear (not shown); the slope gives a barrier height $q\Phi_B^J = 0.53 \pm 0.02$ eV. However, the observed value of the y-axis intercept is smaller than the (A^*S) product by a factor of 10^3 to 10^4. In previous works, similar discrepancies were attributed either to barrier height inhomogeneities in Au-OML-n-Si diodes[18] or to pinholes in Au—alkylthiol—Au systems.[13] Such hypothesis are not necessary; here, we assume that the effective transport area is equal to the geometrical contact area, S, and that the saturation current, $I_s = A^*ST^2\exp(-\beta_T^0 d_T)\exp\left(-\frac{q\Phi_B^J}{kT}\right)$, is attenuated by the tunnel barrier transparency factor, $\exp(-\beta^0 d_T)$, seen by electrons injected above the TE barrier. In this regime, since the voltage drop over the tunnel barrier is small ($V_{TU} \ll V$ as shown in Fig. 7(b)), we can assume that β is independent of applied bias ($\beta(V) \approx \beta^0$). Therefore, the effective barrier height is

$$q\Phi_{EFF} = q\Phi_B^J + kT\beta^0 d_T, \quad (6)$$

where $\beta^0 = 2\left(2m^*\Phi_T/\hbar^2\right)^{\frac{1}{2}}$ is the inverse attenuation length at zero applied bias, $\hbar$ the reduced Planck's constant, and m^* the effective mass of electrical carriers in the OML. Indeed, a plot of the effective barrier height vs temperature (inset of Fig. 3) shows a linear $\Phi_{EFF}(T)$ variation. Note that the positive slope obtained in $\Phi_{EFF}(T)$ plots, in the 243-293 K range, cannot be explained by the small variations of Si band gap $dE_G/dT = -2.4 \times 10^{-4}$ eV.K^{-1} [Ref. 44] and electron affinity $d\chi/dT \approx +1 \times 10^{-4}$ eV.K^{-1} [Ref. 45] which would both produce a small negative slope.

The y-axis intercept is the semiconductor barrier height, $q\Phi_B^I \approx 0.53 \pm 0.05$ eV and the slope provides the tunnel attenuation factor, $\beta^0 d_T = 13.5 \pm 0.2$, of the C_{12} junction (Table I). Using the optical OML thickness (d_T= 1.45 nm) and neglecting image force effects, we obtain $\beta^0 = 0.93 \pm 0.06$ Å^{-1}; this value is consistent with $\beta \approx 0.87 \pm 0.1$ Å^{-1} in Hg-alkanethiol-Ag junctions[46] but it is slightly higher than $\beta^0 \approx 0.65$ Å^{-1} in junctions with a covalent Si-C bonded interface on *n*-type Si.[11] This physical value of β^0 justifies *a posteriori* the hypothesis made in the derivation of Φ_{EFF} (Eq. (6)).

In the literature, most previous values of the tunnel attenuation factor were obtained at room temperature using junctions grafted with variable chain length (d_T); since the structure dependent β^0 values in these "nominally identical" junctions may be affected by different coverage and different structural ordering,[8] we believe that β^0 values derived from the temperature dependence of $J(V)$ in rectifying devices are more reliable than those derived from the length dependence analysis.

In a second step, we study the current-voltage characteristics in the forward bias regime up to 2 V. The knee observed at $V \approx 0.5$ V cannot be solely explained by a limitation due to the series resistance. In the bias range 0.5–1.5 V, since the resistance of the forward biased Schottky barrier vanishes, tunneling through the Hg-OML-n-Si junction should be the limiting transport mechanism.[7,8,11] To model self-consistently the current density $J(V)$, we assume that the current is constant throughout the junction and that the applied voltage, V, is the sum of potential drops on different parts of the device connected in series, $V = V_{TE} + V_{TU} + V_S$. Here, the role of interface states is included in the ideality factor, n. The potential drop on the tunnel barrier, V_{TU}, is related to the current density according to the Simmons model,[24] often used to describe transport through molecular junctions

$$J(V_{TU}) = \frac{G_0}{d_T^2}\left\{\left(\Phi_T - \frac{V_{TU}}{2}\right)\exp\left[-\beta^0 d_T\left(1 - \frac{V_{TU}}{2\Phi_T}\right)^{\frac{1}{2}}\right] - \left(\Phi_T + \frac{V_{TU}}{2}\right)\exp\left[-\beta^0 d_T\left(1 + \frac{V_{TU}}{2\Phi_T}\right)^{\frac{1}{2}}\right]\right\}, \quad (7)$$

where G_0 is related to the charge density availability for tunneling from the metal or from the semiconductor. In the original Simmons work for metal–insulator–metal (MIM) tunnel junctions, $G_0 = 6.2 \times 10^{-6}\ \Omega^{-1}$ (here, J is in A.cm^{-2}, d_T in cm, and Φ_T in Volt). The potential drop, $V_{TE} = n\Phi_{EFF} + (nkT/q)\mathrm{Ln}[J(V)/A*T^2]$, responsible for changes in the thermionic emission barrier is derived from Eq. (5) and the voltage drop due to series resistance is $V_S = R_S J(V) S$.

Using Φ_{EFF} and n values fitted in the low bias regime (where $V_{TU} \approx V_S \approx 0$) and $\beta^0 d_T$ value as fixed parameters, fitting a $J(V)$ characteristic with (G_0, Φ_T, R_S) as adjustable parameters is performed in a wide range of forward applied bias (typically 0.3–2 V). In practice, starting from guess parameters (G_0, Φ_T, R_S) and an arbitrary set of V_{TU} values, the corresponding $J_{TU} = J_{CALC}$ values are obtained using Eq. (7), and $V_{TE}(J_{CALC})$ and $V_S(J_{CALC})$values are further derived. The excellent fit quality, over a current variation of eight decades, is also observed in $G(V) = dJ/dV$ and in the normalized differential conductance (dLnJ/dLnV)[17] (inset in Fig. 7(a)). Fitting parameters (G_0, Φ_T) of the Hg//$C_{12}H_{25} - n$ Si junction are summarized in Table I; they are found to be weakly dependent on temperature, e.g., for six fitting runs of $J(V, T)$ data at different temperatures (243-293 K) with fixed $\beta^0 d_T = 13.5$, the fitted G_0 values vary randomly within a factor of 2.2 and $\Phi_T = 0.51 \pm 0.02$eV. In this T range, $R_S(T)$ decreases from 350 Ω to 200 Ω.

Interestingly, $G_0 = 2.5 \times 10^{-10}\ \Omega^{-1}$ is four decades smaller than the G_0 value ($6.2 \times 10^{-6}\ \Omega^{-1}$) in the original Simmons model for a tunnel barrier between metal electrodes. It has been emphasized that some strong assumptions

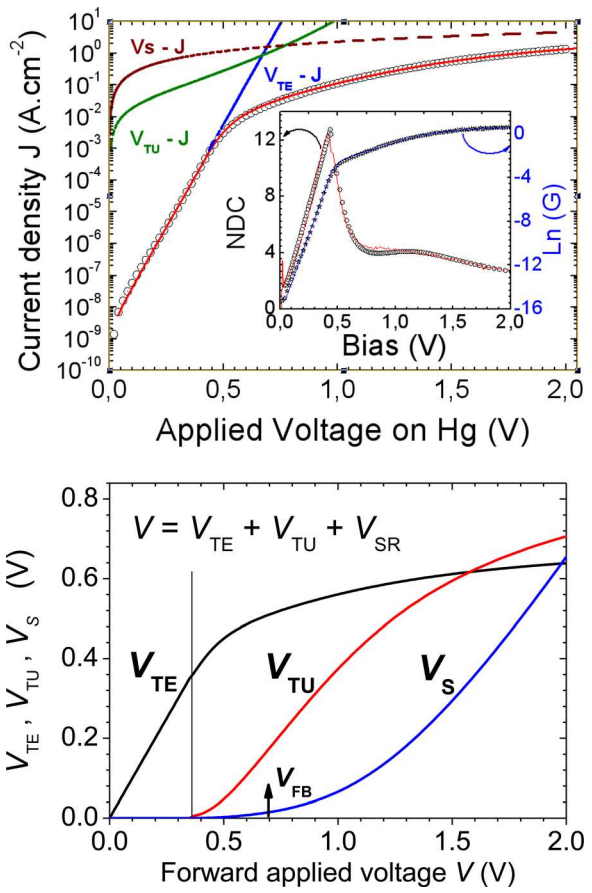

FIG. 7. (Color online) (a) Analysis of $J(V)$ for the Hg//$C_{12}H_{25}$ – n-Si junction (293 K) showing the voltage drop on the tunnel barrier (V_{TU}-J), the thermionic emission contribution (V_{TE}-J),and the series resistance voltage drop (V_S-J). The fit quality is illustrated by LnG and NDC = dLnJ/dLnV vs V plots (inset). (b) Applied voltage partition $V = V_{TE} + V_{TU} + V_S$ in the forward regime.

of the Simmons model, such as the definition of equal longitudinal and transverse effective masses is probably wrong in anisotropic alkyl monolayers.[19] Since the current flows through identical molecules with little cross-talk between them, this should translate into a large m_T value for transport across the molecules and a lower m_L value for transport along the backbone. However, the modified Simmons equation in Ref. 19 gives a higher prefactor value which cannot explain our fitted G_0 value. Alternatively, relatively few metal states may be available for the conduction band electrons in the semiconductor, as a consequence of selection rules based on energy-conservation and transverse momentum conservation in the tunnel transition.[47,48]

In addition, the fitted tunnel barrier height, $\Phi_T = 0.51$ eV, is quite low; this might be a consequence of the image charge effect, which tends to round the corners of the rectangular barrier, reducing both the barrier height and the effective thickness of the barrier.[49] However, inclusion of this additional parameter in a transport model would require an independent determination of the molecular layer dielectric permittivity, which is beyond the scope of this paper.

Although other limitations of the Simmons model have been considered,[13] along with the possible breakdown of the Wentzel-Kramers-Brillouin (WKB) approximation for ultra thin tunnel barriers,[50] the interest of Eq. (7) in this work is that it basically captures the physics of the rectangular tunnel barrier, namely the decrease of the average barrier height with bias V_{TU} applied on the tunnel barrier, in a closed-form expression with a limited number of parameters.

Figure 7(b) shows the voltage partition between the tunnel barrier, the TE barrier, and the series resistance. The onset of V_{TU} occurs near $V = 0.4$ V, which is consistent with the $n(V)$ plot (Fig. 6(a)). In the TB limited regime, near flat band voltage, the applied bias is shared between the tunnel barrier and the thermionic emission barrier. The effective value, $(\Phi_M - X_{Si})_{EFF}$, including the effect of interface Si-C dipoles is deduced from this voltage partition. At the flat band voltage, $V_{FB} = 0.68$ V and the voltage drop over the insulator $V_{TU} = -V_I = 0.18$ V (Figure 7(b)). Using $V_N = 0.30$ V at 293 K, $(\Phi_M - X_{Si})_{EFF} = 0.80$ eV is deduced from Eq. (1); this experimental value is larger than the ideal value $(q\Phi_M - qX_{Si}) = 0.44$ eV, where $q\Phi_M$ is the metal work function (4.49 eV for Hg) and qX_{Si} is the electron affinity of Si (4.05 eV). This difference (0.36 eV) corresponds to a decrease of the effective X_{Si} value; it is consistent with the formation of molecular dipoles at the interface, as observed using synchrotron photoemission.[51]

In summary, the barrier height $\Phi_B^C = (1/n)V_{FB} + V_N = 0.77 \pm 0.03$ eV (Eq. 2(b)) is derived from the Mott-Schottky plot of the capacitance. The latter value of Φ_B^C is larger than the value, $\Phi_B^J = 0.53 \pm 0.02$ V, derived from the temperature dependence of $J(V, T)$ in the forward bias regime (Eq. (5)). Again, this discrepancy supports the assumption made in the interpretation of experimental $n(V)$ results, namely the existence of a distribution of barrier heights[38–40] due to surface potential fluctuations arising from some inhomogeneous distribution of dipoles or charged defects.

C. Analysis of the reverse bias regime

On the basis of dc transport in Hg//alkyl – *n* Si junctions with variable alkyl molecule length, showing that the reverse bias regime is basically independent of the molecular layer,[16] it has been argued previously that transport is minority carrier controlled for reverse bias and low forward bias.

In this work, several reverse bias characteristics support a generation recombination (GR) mechanism: (a) the saturation current $J_{REV}(293K) = 4 \times 10^{-8}$A.cm^{-2} in this C_{12} junction is identical to Ref. 16 and consistent with a generation recombination current $J_{GR} = 2 \times 10^{-8}$A.cm^{-2} expected from the GR model[35,41] where $J_{GR} = qw_{MAX}\frac{n_i}{\tau_0}$, τ_0 is the recombination lifetime in the depletion region ($\tau_0 = 10^{-5}$ s in Czochralski silicon[52,53]), n_i the intrinsic carrier density ($n_i \approx 10^{10}$ cm^{-3} at 293 K), and w_{MAX} ($\approx 10^{-4}$ cm) the maximum width of the depletion region. (b) the response time $\tau_R = 0.3$ s deduced from admittance data at 293 K is close to the theoretical value, $\tau_R = 0.1$ s, of the minority carrier response time[34] $\tau_R \approx \frac{1}{\sqrt{2}}\frac{N_D}{n_i}\tau_0$, estimated using the dopant density $N_D = 1.5 \times 10^{14}$ cm^{-3}. (c) both $E_{ACT}(\tau_{REV}) = 0.54 \pm 0.02$ eV and $E_{ACT}(J_{REV}) \approx 0.58 \pm 0.05$ eV are close to half the Si bandgap ($E_G/2$), as expected from the activated behaviour of n_i.

However, the bias dependence of the reverse current is not consistent with the exponent 1/2 expected for a generation-recombination current.[35] Experimental J_{REV} data analysis with a log J_{REV} vs log $(V_{FB} - V)$ plot, using the flat band voltage derived from the Mott-Schottky plot, reveals an Ohmic behavior (the slope is 1.0 ± 0.1, not shown) for all bias values ($V > -2$ V) at low temperatures (243−263 K) and for moderate reverse bias ($V > -1$ V) at higher temperatures (283 K).

D. Distribution of interface states

The ac response of interface traps due to the modulation of their average occupation is described by a parallel capacitance—resistance circuit in parallel with the space charge layer capacitance (inset of Fig. 4(a)). The energy distribution of the density of interface states, $D_S(E_C - E_T)$, in the upper half of the band gap can be derived from either the capacitance or the conductance parts of the admittance. In the latter case, for Hg//$C_{12}H_{25}$ –*n*-Si(111) junctions, the low frequency conductance masks the response of electrically active interface defects; after subtraction of this dc conductance, a broad maximum is observed in a (G/ω) *vs* $(\omega/2\pi)$ plot. Similarly, a step appears in $C(\omega)$ and occurs at the same frequency, $(\omega_{MAX}/2\pi)$. With increasing forward bias, as the surface Fermi level approaches the SC conduction band, ω_{MAX} shifts towards higher values (not shown) as expected for carriers emitted from interface traps (at $E_T = E_{FS}$) to the conduction band.

Alternatively, $D_S(E_C - E_T)$ can be obtained from the low-high frequency capacitance response, $D_S = (C_{LF} - C_{HF})/qS$; this approximation holds because the insulator capacitance, C_I, is very large.[34] Using $C(V)$ plots of the Hg//$C_{12}H_{25}$ – *n* Si junction at 100 Hz and 1 MHz. respectively, this method is sensitive to traps with $(\omega_{MAX}/2\pi)$ located within this frequency

window. The trap depth (at $E_T = E_{FS}$) is derived from Eq. (1): $(E_C - E_T)/q = \Psi_S(V) + V_N = (\Phi_M - X_{Si})_{EFF} + V_{TU} - V$ using $V - V_{TU} \approx V_{TE}$ given in Figure 7(b) and $(\Phi_M - X_{Si})_{EFF} = 0.77$ eV.

Figure 7 shows that the density of interface states increases as the interface Fermi level approaches the conduction band, from $D_S \approx 1 \times 10^{10}$ eV^{-1}.cm^{-2} near mid-gap to 7×10^{12} eV^{-1} cm^{-2} at E_C–0.30 eV (corresponding to V_{FB} at 293 K). This low interface states density, $D_S < 10^{11}$ eV^{-1} cm^{-2}, near midgap indicates a good passivation of dangling bonds at the dodecyl *n*-Si interface, which is better than the values ($D_S \approx 4 \times 10^{11}$ eV^{-1} cm^{-2}) reported previously for octadecyl *n*-Si junctions.[23]

The validity of D_S values obtained at forward bias near flat bands should be taken with care. We have observed (Fig. 4(a)) that the measured low frequency capacitance is larger than the expected capacitance value of the molecular insulator, $C_I = 9$ nF. Hence, D_S values derived from the low-high frequency method (triangles in Fig. 8) are overestimated for large dc currents in thin tunnel MIS junctions. To estimate the magnitude of such dc current effect, we have used a model proposed by Gomila[26] who considered coupled kinetic equations for the charge exchange between the interface states, the metal and the semiconductor in a tunnel MIS junction. The conductance G and capacitance C were computed in the forward bias regime (using Eqs. (20) and (21) in Ref. 26) at low frequency (100 Hz) and with a small value of the microscopic time constant of the traps ($\tau = 10^{-7}s$); in this preliminary study, we find that the dependence of the response time τ_R^{CALC} vs bias is very sensitive to the D_S value. Figure 9 simulations were obtained with variable D_S values, using experimental $J(V)$ data at 293 K (Fig. 3), and assuming $C_I = 9$ nF and $C_{SC} = 10$ pF. The results show that the magnitude of D_S does not exceed 2×10^{11} eV^{-1}.cm^{-2}. Hence, the exponential increase in $D_S(E_C - E_T)$ near the conduction band shown in Fig. 8 is an artefact due to the large dc current density. In contrast, the calculations using the Gomila–Rubi model confirm the validity of $D_S$values ($D_S < 2 \times 10^{11}$ eV^{-1} cm^{-2}) near mid-gap.

The electrically active interface states near midgap are tentatively attributed to dangling bonds at surface Si atoms.

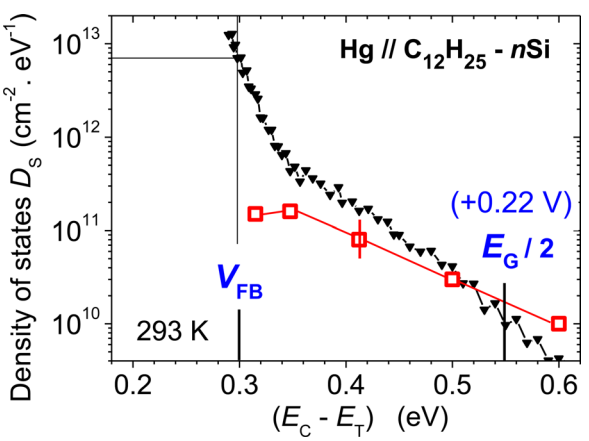

FIG. 8. (Color online) Energy dependence of the density of interface states $D_S(E_C - E_T)$ derived from the low-high frequency capacitance (black triangles) and from simulations using the Gomila-Rubi model (red squares).

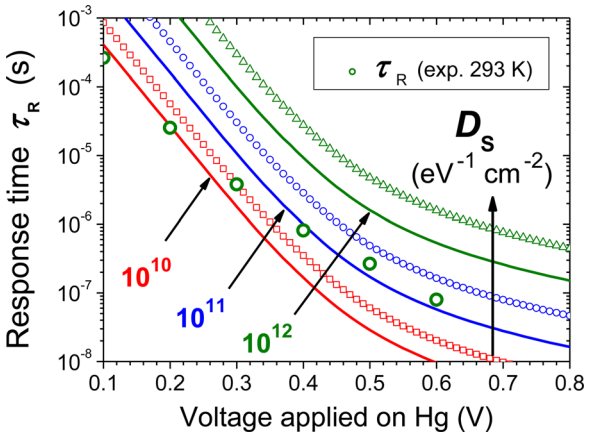

FIG. 9. (Color online) Tunnel junction response time: experimental values at 293 K (circles) and simulation taking into account the experimental $J(V)$ and variable density of interface states D_S from 1×10^{10} to 3×10^{12} eV^{-1} cm^{-2} (lines: Gomila model[26]).

Due to sterical constraints, the density of surface sites which are not grafted with $C_{12}H_{25}$ molecules is larger than 4×10^{14} cm^{-2} (≈50% of surface Si atom density) even in the case of a closely packed molecular layer[54]; the low density of electrically active interface states, $D_S < 10^{11}$ eV^{-1} cm^{-2}, found in this study thus requires that (1) the Si dangling bonds are fully passivated by the hydrogenation process and (2) that the Si-H bonding is not disrupted by the grafting process of 1-alkene molecules. However, ageing in air affects the midgap density which typically rises to the high 10^{11} eV^{-1}.cm^{-2} range; future work might address the role of molecular coverage in the kinetics of this oxidation reaction.

Finally, considering Eq. (4), an apparent discrepancy can be noticed between the large ideality factor value ($n = 1.46$ at 293 K) found in this work and the small density of interface states ($D_S < 10^{11}$ eV^{-1}.cm^{-2}) obtained in the same bias range. Thus, another origin for high n values must exist, e.g., barrier height inhomogeneities (due either to dipoles or charged interface traps) or tunnel barrier thickness inhomogeneities may contribute to the large apparent n values found in this work. This interpretation of high n values is supported by the discrepancy between the barrier heights obtained from $C(V)$ and $I(V)$ characteristics, as shown by modelling studies.[38–40]

V. CONCLUSION

Electrical transport mechanisms in rectifying Hg// $C_{12}H_{25}$ – *n* Si(111) junctions with nanometer thick molecular insulator have been investigated using the *temperature dependence* of current density $J(V, T)$ and admittance $Y(V, T, \omega)$ characteristics. With low doped *n*–type silicon, $J(V)$ characteristics show a strong rectification ($R \geq 10^6$) with a limitation of the current by the tunnel barrier and series resistance in the forward bias regime. The carrier dynamics in the MIS tunnel junction (tunnel and thermionic emission barriers, interface traps) has been investigated using a frequency response analysis (10^{-2}-10^7 Hz). At room temperature, the device response time τ_R covers seven decades (1 to

10^{-7} s) as the applied bias is swept from depletion to near flat band voltage V_{FB}.

The voltage partition over the junction was obtained from $J(V, T)$ characteristics, with an excellent fitting over the full bias range corresponding to a current variation over eight decades. This work shows that the temperature dependence of the effective barrier height in the thermionic emission regime is crucial to obtain accurate values of barrier height, Φ_B, in the SC and tunnel attenuation factor, $\exp(-\beta^0 d_T)$. We argue that β^0 values derived from the temperature dependence of $J(V)$ in rectifying devices are more reliable than β^0 derived from length dependence analysis. Complementary studies with different molecular layers are currently performed. The low tunnel barrier height $\Phi_T = 0.51$ eV could result from the neglected image charge effects. The low value of the fitted current density prefactor, G_0, reveals the role of tunneling selection rules in MIS junctions. However, the assumptions used to derive the current density prefactor in the Simmons model have been revisited recently[19] and deserve more detailed investigation.

The density distribution of defects localized at the $C_{12}H_{25} - n$ Si interface has been deduced from admittance data (low-high frequency method) and from a simulation of the response time $\tau_R(V)$ using Gomila's model for a non equilibrium tunnel junction. This preliminary study shows that D_S values derived from the low-high frequency method are overestimated for large dc currents in thin tunnel MIS junctions; more accurate values require further simulations, e.g., using the Gomila-Rubi model.[25,26]

The low density of electrically active defects near midgap ($D_S < 2 \times 10^{11}$ eV^{-1} cm^{-2}) indicates a good passivation of dangling bonds at the dodecyl—*n* Si interface. Future improvement of molecular tunnel junction devices will require a better control of lateral homogeneity of the molecular layer.

ACKNOWLEDGMENTS

Arnaud Le Pottier is gratefully acknowledged for designing the sample holder for electrical measurements.

[1]D. K. Aswal, S. Lenfant, D. Guerin, J. V. Yakhimi, and D. Vuillaume, Anal. Chim. Acta **568**, 84 (2006).
[2]D. Vuillaume, C. R. Phys. **9**, 78 (2008).
[3]A. Vilan, O. Yaffe, A. Biller, A. Salomon, A. Kahn, and D. Cahen, Adv. Mater. **22**, 140 (2010).
[4]O. Seitz, A. Vilan, H. Cohen, J. Hwang, M. Haeming, A. Schoell, E. Umbach, A. Kahn, and D. Cahen, Adv. Funct. Mater. **18**, 2102 (2008).
[5]M. R. Linford, P. Fenter, P. M. Eisenberger, and C. E. D. Chidsey, J. Am. Chem. Soc. **117**, 3145 (1995).
[6]R. Boukherroub, Curr. Opin. Solid State Mater. Sci. **9**, 66 (2005).
[7]H. Sabbah, S. Ababou-Girard, A. Zebda, D. David, B. Fabre, S. Députier, A. Perrin, M. Guilloux-Viry, F. Solal, and C. Godet, Diamond Relat. Mater. **18**, 1074 (2009).
[8]Y. Selzer, A. Salomon, and D. Cahen, J. Phys. Chem. B **106**, 10432 (2002).
[9]Y. L. Liu and H. Z. Yu, J. Phys. Chem. B **107**, 7803 (2003).
[10]E. J. Faber, L. C. P. M. de Smet, W. Olthuis, H. Zuilhof, E. J. R. Sudholter, P. Bergveld, and A. Van den Berg, Chem. Phys. Chem. **6**, 2153 (2005).
[11]A. Salomon, T. Boecking, C. K. Chan, F. Amy, O. Girshevitz, D. Cahen, and A. Kahn, Phys. Rev. Lett. **95**, 266807 (2005).
[12]S. Maldonado, K. E. Plass, D. Knapp, and N. S. Lewis, J. Phys. Chem. C **111**, 17690 (2007).
[13]A. Vilan, J. Phys. Chem. C **111**, 4431 (2007).
[14]A. Salomon, T. Boecking, O. Seitz, T. Markus, F. Amy, C. K. Chan, W. Zhao, D. Cahen, and A. Kahn, Adv. Mat. **19**, 445 (2007).
[15]M. Furuhashi, A. Omura, Y. Yamashita, K. Mukai, J. Yoshinobu, K. Akagi, and S. Tsuneyuki, Jpn. J. Appl. Phys. **48**, 055003 (2009).
[16]O. Yaffe, L. Scheres, S. R. Puniredd, N. Stein, A. Biller, R. H. Lavan, H. Shpaisman, H. Zuilhof, H. Haick, D. Cahen, and A. Vilan, Nano Lett. **9**, 2390 (2009).
[17]C. Godet, A. Fadjie, S. Ababou-Girard, and F. Solal, Appl. Phys. Lett. **97**, 132105 (2010).
[18]I. Taşçioglu, U. Aydemir, and S. Altindal, J. Appl. Phys. **108**, 064506 (2010).
[19]A. W. Ghosh, *Comprehensive Semiconductor Science and Technology* (Elsevier, Amsterdam, 2011), Chap. 5.09, pp. 383-447.
[20]W. J. Royea, A. Juang, and N. S. Lewis, Appl. Phys. Lett. **77**, 1988 (2000).
[21]D. Michalak and N. S. Lewis, Appl. Phys. Lett. **80**, 4458 (2002).
[22]A. Lehner, F. Kohl, S. A. Franzke, T. Graf, M. S. Brandt, and M. Stutzmann, Appl. Phys. Lett. **82**, 565 (2003).
[23]S. Kar, Appl. Surf. Sci. **252**, 3961 (2006).
[24]J. G. Simmons, J. Appl. Phys. **34**, 1793 (1963).
[25]G. Gomila and J. M. Rubi, J. Appl. Phys. **81**, 2674 (1997).
[26]G. Gomila, J. Phys. D: Appl. Phys. **32**, 64 (1999).
[27]B. Fabre, S. Cordier, Y. Molard, C. Perrin, S. Ababou-Girard, and C. Godet, J. Phys. Chem. C **113**, 17437 (2009).
[28]C. P. Wade and C. E. D. Chidsey, Appl. Phys. Lett. **71**, 1679 (1997).
[29]B. Fabre, S. Ababou-Girard, and F. Solal, J. Mater. Chem. **15**, 2575 (2005).
[30]S. Cordier, B. Fabre, Y. Molard, A. B. Fadjie-Djomkam, N. Tournerie, A. Ledevna, N. G. Naumov, A. Moréac, P. Turban, S. Tricot, S. Ababou-Girard, and C. Godet, J. Phys. Chem. C **114**, 18622 (2010).
[31]A. Faucheux, A. C. Gouget-Laemmel, C. Henry de Villeneuve, R. Boukherroub, F. Ozanam, P. Allongue, and J. N. Chazalviel, Langmuir **22**, 153 (2006).
[32]C. J. Powell and A. Jablonski, NIST Electron Inelastic-Mean-Free-Path, Database version 1.1 (2000).
[33]X. Wallart, C. Henry de Villeneuve, and P. Allongue, J. Am. Chem. Soc. **127**, 7871 (2005).
[34]E. H. Nicollian and J. R. Brews, *MOS (Metal Oxide Semiconductor) Physics and Technology* (Wiley, New York, 1982).
[35]A. Y. C. Yu and E. H. Snow, J. Appl. Phys. **39**, 3008 (1968).
[36]S. Kar, Appl. Phys. Lett. **25**, 587 (1974).
[37]H. C. Card and E. H. Rhoderick, J. Phys. D: Appl. Phys. **4**, 1589 (1971).
[38]J. P. Sullivan, R. T. Tung, M. R. Pinto, W. R. Graham, J. Appl. Phys. **70**, 7403 (1991).
[39]R. T. Tung, Mater. Sci. Eng. R. **35**, 1 (2001).
[40]J. H. Werner and H. H. Güttler, J. Appl. Phys. **69**, 1522 (1991).
[41]S. M. Sze, *Semiconductor Devices: Physics and Technology* (Wiley, New York, 1985).
[42]C. Y. Wu, J. Appl Phys. **51**, 3786 (1980).
[43]C. Y. Wu, J. Appl Phys. **53**, 5947 (1982).
[44]Y. P. Varshni, Physica **34**, 149 (1967).
[45]F. G. Allen, J. Phys. Chem. Solids **8**, 119 (1959).
[46]R. E. Holmlin, R. Haag, M. L. Chabinyc, R. F. Ismagilov, A. E. Cohen, A. Terfort, M. A. Rampi, and G. M. Whitesides, J. Am. Chem. Soc. **123**, 5075 (2001).
[47]P. V. Gray, Phys. Rev. A **140**, 179 (1965).
[48]J. Maserjian and G. P. Petersson, Appl. Phys. Lett. **25**, 50 (1974).
[49]J. G. Simmons, J. Appl. Phys. **35**, 2472 (1964).
[50]J.C. Ranuarez, M.J. Deen, and C.H. Chen, Microel. Rel. **46**, 1939 (2006).
[51]R. Hunger, R. Fritsche, B. Jaeckel, W. Jaegermann, L. J. Webb, and N. S. Lewis, Phys. Rev. B **72**, 045317 (2005).
[52]H. Mathieu, *Physique des Semiconducteurs et des Composants Électroniques* (Masson, Paris, 1998).
[53]F. Shimura, T. Okui, and T. Kusama, J. Appl. Phys. **67**, 7168 (1990).
[54]L. Scheres, M. Giesbers, and H. Zuilhof, Langmuir **26**, 4790 (2010).